INTERNATIONAL JOURNAL OF
NUMERICAL ANALYSIS AND MODELING
Volume 16, Number 5, Pages 767–788

ROBUST AND EFFICIENT MIXED HYBRID DISCONTINUOUS FINITE ELEMENT METHODS FOR ELLIPTIC INTERFACE PROBLEMS

JIANG ZHU AND HÉCTOR ANDRÉS VARGAS POBLETE

Abstract. Because of the discontinuity of the interface problems, it is natural to apply the discontinuous Galerkin (DG) finite element methods to solve those problems. In this work, both fitted and unfitted mixed hybrid discontinuous Galerkin (MHDG) finite element methods are proposed to solve the elliptic interface problems. For the fitted case, the problems can be solved directly by MHDG method. For the unfitted case, the *broken* basis functions (unnecessary to satisfy the jump conditions) are introduced to those elements which are cut across by interface, the weights depending on the volume fractions of cut elements and the different diffusions (or material heterogeneities) are used to stabilize the method, and the idea of the Nitsche's penalty method is applied to guarantee the jumps on the interface parts of cut elements. Unlike the immersed interface finite element methods (IIFEM), the two jump conditions are enforced weakly in our variational formulations. So, our unfitted interface MHDG method can be applied more easily than IIFEM to general cases, particularly when the immersed basis function cannot be constructed. Numerical results on convergence and sensitivities of both interface location within a cut element and material heterogeneities show that the proposed methods are robust and efficient for interface problems.

Key words. Elliptic interface problems, discontinuous Galerkin finite element methods, mixed and hybrid methods, Nitsche's penalty method, sensitivities of interface location and material heterogeneities.

1. Introduction

Interface problems arise frequently in many applications, as for example, in heat and mass transfer, electromagnetic wave propagation, cell and bubble formation, biological science, fluid mechanics and many other practical applications. In these problems, the solution and the flux are usually nonsmooth on interface. Interface problems with fixed interfaces can be solved efficiently by fitted interface methods [7, 5, 10, 20]. In these methods the meshes are constructed to align or approximate to the interface. However, for the moving interface problems, the fitted interface methods are very costly because of the generation of new fitted interface meshes at each time step.

To overcome this difficulty, the unfitted interface methods have been studied. The immersed boundary method was proposed in [29] to model blood flow in the heart. Since then, other unfitted interface methods, such as the immersed interface (finite difference) method [21, 19], the immersed interface finite element method (IIFEM) [23, 24, 15, 17, 18], the ghost fluid method [14, 25, 26], the extended finite element method (XFEM) [28, 4, 37], the Nitsche's penalty method [16, 1, 27], and so on, have been developed. In unfitted interface methods, the meshes are fixed, independent of the interface geometry and the interface usually cuts through cells. Then the moving interface problems can be solved with fixed meshes, without remeshing process.

Received by the editors December 22, 2017 and, in revised form , February 27, 2019.
2000 *Mathematics Subject Classification.* 35R35, 49J40, 60G40.

Because of the discontinuity of the interface problems, it is natural to apply the DG methods to solve those problems. The DG methods were introduced independently in [13, 31, 6]. Since then, numerous DG methods have been developed. Because of the flexibility for mesh and polynomial refinements, localizability, stability and parallelizability, the DG methods have been widely applied to many problems. Recently, a fitted DG method with a priori and a posteriori error estimations for the interface diffusion problem was studied in [10], the hybridizable DG (HDG) method based on [11] was applied to the fitted interface diffusion problem in [20], an unfitted DG method based on Nitsche's penalty method for the interface diffusion problem was introduced and analyzed in [27], and a selective immersed DG method for the interface diffusion problem was proposed in [17]. Besides, the mixed method can be used to get more precise approximation to the flux which is necessary in many applications, particularly for the coupled problems [34, 33, 35, 36, 32, 22]. From computational point of view, a particular advantage of the MHDG method is that it can be formulated and implemented at the element level. This allows to eliminate the primal and flux variables on the element level, then to obtain a global system only for the Lagrange multipliers.

In this work, we propose both fitted and unfitted MHDG methods for elliptic interface problems. For the fitted case, we solve the problems directly by the MHDG methos [13, 2, 8, 9, 11, 12]. For the unfitted case, similarly to the idea presented in[16], we propose the *broken* Raviart-Thomas basis functions (unnecessary to satisfy the jump conditions) to those elements which are cut across by interface, we introduce the weighted averages depending on the volume fractions of cut elements and the material heterogeneities to stabilize the method, and we apply the idea of the Nitsche's penalty method to guarantee the jumps on the interface parts of cut elements. Unlike the IIFEM method, the two jump conditions are enforced weakly in our variational formulations. Thus, our unfitted MHDG method can be applied more easily than IIFEM method to general cases, particularly when the immersed basis function cannot be constructed. Numerical results on convergence and sensitivities of both interface location within a cut element and material heterogeneities show that the proposed methods are robust and efficient for interface problems.

The paper is organized as follows. In section 2, we introduce the elliptic interface model problem, define the notations and the finite element spaces. In section 3, we present the fitted MHDG method and the corresponding numerical results. In section 4, we formulate the unfitted MHDG method. However, numerical results show that the flux on interface cannot be well approximated by the formulation. To get a good approximation to the flux on interface and to guarantee the interface jumps, we introduce two penalty terms to the formulation in section 4.2. As a result we obtain numerically a robust and efficient MHDG method for both cut elements with arbitrary small volume fractions and large material heterogeneities. Finally in section 5 we present some concluding remarks. The numerical analysis of the proposed interface MHDG method should be our next work.

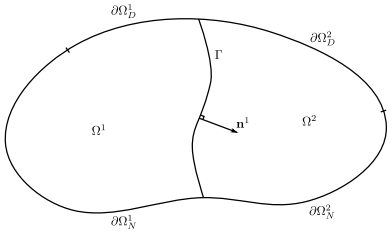

FIGURE 1. Ω is divided by the interface Γ into two disjoint subdomains, Ω^1 and Ω^2. $\partial\Omega_D^i$ and $\partial\Omega_N^i$ $(i = 1, 2)$ are Dirichlet and Neumann boundaries, respectively. $\mathbf{n}^1$ is the outward unit normal vector of Ω^1.

2. Model problem

In this work we consider the following elliptic interface problem:

$$
\left\{\begin{array}{rrcll}
\text{(i)} & -\nabla\cdot(\kappa^i\nabla u^i) & = & f & \text{in } \Omega^i,\ i=1,2,\\
\text{(ii)} & u^i & = & g_D^i & \text{on } \partial\Omega_D\cap\partial\Omega^i,\\
\text{(iii)} & -\kappa^i\nabla u^i\cdot\mathbf{n}^i & = & g_N^i & \text{on } \partial\Omega_N\cap\partial\Omega^i,\\
\text{(iv)} & [\![u]\!] = u^1\mathbf{n}^1+u^2\mathbf{n}^2 & = & s_D\mathbf{n}^1 & \text{on } \Gamma,\\
\text{(v)} & -[\![\kappa\nabla u]\!] = -\left(\kappa^1\nabla u^1\cdot\mathbf{n}^1+\kappa^2\nabla u^2\cdot\mathbf{n}^2\right) & = & s_N & \text{on } \Gamma,
\end{array}\right. \tag{1}
$$

where $\Omega\subset\mathbb{R}^d$ is a bounded domain with Lipschitz boundary $\partial\Omega=\partial\Omega_D\cup\partial\Omega_N$ such that $\partial\Omega_D\cap\partial\Omega_N=\emptyset$. The two subdomains Ω^1 and Ω^2, satisfy $\Omega^1\cap\Omega^2=\emptyset$, $\overline{\Omega}=\overline{\Omega^1}\cup\overline{\Omega^2}$ and the interface $\Gamma=\overline{\Omega^1}\cap\overline{\Omega^2}$, $\kappa\in L^\infty(\Omega)$ is a positive diffusion function, with possible large jumps across subdomain boundaries, $\kappa^i=\kappa\,|_{\Omega^i}\in C(\overline{\Omega^i})$, $f\in L^2(\Omega)$, $g_D\in H^{1/2}(\partial\Omega_D)$, $g_N\in L^2(\partial\Omega_N)$, $s_D\in H^{1/2}(\Gamma)$, $s_N\in L^2(\Gamma)$ and $\mathbf{n}^i$ denotes the outward unit normal vector of Ω^i, see Figure 1 for details.

Let $\boldsymbol{\sigma}^i=-\kappa^i\nabla u^i$ the diffusive flux, then the model problem (1) can be written in mixed form as:

$$
\left\{\begin{array}{rrll}
\text{(i)} & \frac{1}{\kappa^i}\boldsymbol{\sigma}^i+\nabla u^i=0 & & \text{in } \Omega^i,\ i=1,2,\\
\text{(ii)} & \nabla\cdot\boldsymbol{\sigma}^i=f & & \text{in } \Omega^i,\ i=1,2,\\
\text{(iii)} & u^i=g_D^i & & \text{on } \partial\Omega_D\cap\partial\Omega^i,\\
\text{(iv)} & \boldsymbol{\sigma}^i\cdot\mathbf{n}^i=g_N^i & & \text{on } \partial\Omega_N\cap\partial\Omega^i,\\
\text{(v)} & [\![u]\!]=u^1\mathbf{n}^1+u^2\mathbf{n}^2=s_D\mathbf{n}^1 & & \text{on } \Gamma,\\
\text{(vi)} & [\![\boldsymbol{\sigma}]\!]=\left(\boldsymbol{\sigma}^1\cdot\mathbf{n}^1+\boldsymbol{\sigma}^2\cdot\mathbf{n}^2\right)=s_N & & \text{on } \Gamma.
\end{array}\right. \tag{2}
$$

2.1. Finite element approximation. Let $\mathcal{T}_h$ be a regular triangulation of Ω, see Figure 2. For each element $T\in\mathcal{T}_h$, we denote by ∂T the boundary of T, set $\partial\mathcal{T}_h=\{\partial T: T\in\mathcal{T}_h\}$. Denote by $\mathcal{E}_h$ the set of all edges of $\mathcal{T}_h$, $\mathcal{E}_h^I$ is the set of all interior edges, $\mathcal{E}_h^D$ and $\mathcal{E}_h^N$ are the sets of all boundary edges belonging to the Dirichlet and Neumann boundaries $\partial\Omega_D$ and $\partial\Omega_N$, respectively. Then we have $\mathcal{E}_h=\mathcal{E}_h^I\cup\mathcal{E}_h^D\cup\mathcal{E}_h^N$. Furthermore, denote h_e the diameter of $e\in\mathcal{E}_h$, $e^i=e\cap\Omega^i$. $|T|$ is the area/volume of $T\in\mathcal{T}_h$. $T^i=T\cap\Omega^i$ and $\Gamma_T=T\cap\Gamma$. We define

$$
\mathcal{T}_h^i=\{T: T\in\mathcal{T}_h; |T^i|>0\},\quad \mathcal{T}_h^0=\mathcal{T}_h^1\cap\mathcal{T}_h^2, \tag{3}
$$

$$
\mathcal{E}_h^i=\{e: e\in\mathcal{E}_h; |e^i|>0\},\quad \mathcal{E}_h^0=\mathcal{E}_h^1\cap\mathcal{E}_h^2, \tag{4}
$$

and the discontinuous finite element spaces

$$
\mathcal{V}_h=\mathcal{V}_h^1\times\mathcal{V}_h^2,\qquad \mathcal{U}_h=\mathcal{U}_h^1\times\mathcal{U}_h^2,\qquad \mathcal{M}_h=\mathcal{M}_h^1\times\mathcal{M}_h^2, \tag{5}
$$

$$
\begin{aligned}
\mathcal{V}_h^i &= \left\{ \boldsymbol{\tau}_h^i : \boldsymbol{\tau}_h^i \in [L^2(\Omega^i)]^d : \boldsymbol{\tau}_h^i \,|_T \,; \in \mathcal{RT}_k(T),\ \forall\, T \in \mathcal{T}_h^i \right\}, \\
\mathcal{U}_h^i &= \left\{ v_h^i : v_h^i \in L^2(\Omega^i) : v_h^i \,|_T \,; \in \mathcal{P}^k(T),\ \forall\, T \in \mathcal{T}_h^i \right\}, \\
\mathcal{M}_h^i &= \left\{ \mu_h^i : \mu_h^i \in L^2(\mathcal{E}_h^i) : \mu_h = 0 \text{ on } \partial\Omega_D, \mu_h^i \,|_e \ \in \mathcal{P}^k(e),\ \forall\, e \in \mathcal{E}_h^i \right\},
\end{aligned} \tag{6}
$$

where $\mathcal{P}^k(T)$ denotes the space of polynomials of degree $\leq k$ on T and $\mathcal{RT}_k(T)$ denotes the Raviart-Thomas space on T [30], defined by

$$
\mathcal{RT}_k(T) = \left[\mathcal{P}^k(T)\right]^d + \mathbf{x}\mathcal{P}^k(T). \tag{7}
$$

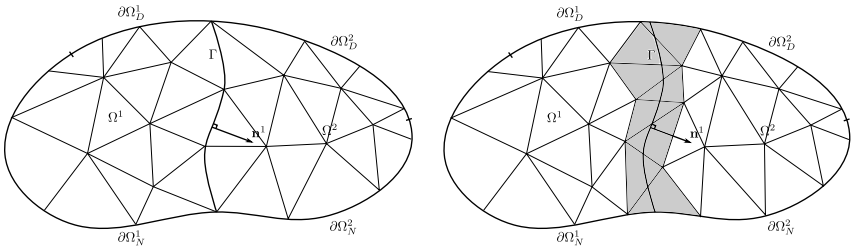

(A) Fitted mesh (B) Unfitted mesh

FIGURE 2. Fitted and unfitted triangulations for the domain Ω. In the fitted case the mesh is aligned with the interface Γ, then $\mathcal{T}_h^0 = \emptyset$ and $\mathcal{E}_h^0 = \emptyset$. For the unfitted case, Γ cuts arbitrarily the elements because the mesh is not aligned with the interface. The grey zone corresponds to the set $\mathcal{T}_h^0$, i.e. the set of elements crossed by the interface. In the unfitted case $\mathcal{T}_h^0 \neq \emptyset$ and $\mathcal{E}_h^0 \neq \emptyset$ in general.

For $\boldsymbol{\sigma}_h = \left(\boldsymbol{\sigma}_h^1, \boldsymbol{\sigma}_h^2\right) \in \mathcal{V}_h$ and $u_h = \left(u_h^1, u_h^2\right) \in \mathcal{U}_h$. We define the jumps on Γ_T as

$$
[\![\boldsymbol{\sigma}_h]\!] = \boldsymbol{\sigma}_h^1 \cdot \mathbf{n}^1 + \boldsymbol{\sigma}_h^2 \cdot \mathbf{n}^2, \quad [\![u_h]\!] = u_h^1 \mathbf{n}^1 + u_h^2 \mathbf{n}^2 \quad \text{on } \Gamma_T \text{ for } T \in \mathcal{T}_h^0, \tag{8}
$$

the volume and edge inner products as

$$
(u_h, v_h)_{\mathcal{T}_h} = \sum_{T \in \mathcal{T}_h} (u_h, v_h)_T, \quad (u_h, v_h)_T = \left(u_h^1, v_h^1\right)_{T^1} + \left(u_h^2, v_h^2\right)_{T^2}, \tag{9}
$$

$$
\langle u_h, v_h \rangle_{\partial\mathcal{T}_h} = \sum_{T \in \mathcal{T}_h} \langle u_h, v_h \rangle_{\partial T}, \quad \langle u_h, v_h \rangle_{\partial T} = \langle u_h^1, v_h^1 \rangle_{\partial T \cap T^1} + \langle u_h^2, v_h^2 \rangle_{\partial T \cap T^2}. \tag{10}
$$

For a piecewise constant κ, we define

$$
\kappa\,(u_h, v_h)_{\mathcal{T}_h} = \sum_{T \in \mathcal{T}_h} (\kappa u_h, v_h)_T \quad \text{and} \quad \kappa \langle u_h, v_h \rangle_{\partial\mathcal{T}_h} = \sum_{T \in \mathcal{T}_h} \langle \kappa u_h, v_h \rangle_{\partial T} \tag{11}
$$

3. Fitted MHDG method

For a fitted mesh $\mathcal{T}_h$ of Ω. Multiplying (2.i) and (2.ii) by test functions $\boldsymbol{\tau}_h$ and v_h respectively, integrating on element $T \in \mathcal{T}_h$, and applying the Green formula in the first equation, we obtain

$$
\frac{1}{\kappa}\,(\boldsymbol{\sigma}_h, \boldsymbol{\tau}_h)_T - (u_h, \nabla \cdot \boldsymbol{\tau}_h)_T + \langle \widehat{u}_h, \boldsymbol{\tau}_h \cdot \mathbf{n} \rangle_{\partial T} = 0, \tag{12}
$$

$$
-\,(\nabla \cdot \boldsymbol{\sigma}_h, v_h)_T = -\,(f, v_h)_T\,. \tag{13}
$$

Now, to capture the jump condition for the solution on the interface, $\widehat{u}_h$ is defined in terms of $\lambda_h \in \mathcal{M}_h$ as follows:

$$
\widehat{u}_h = \begin{cases} \lambda_h + s_D, & \text{if } e \cap \Gamma \neq \emptyset, \text{ for } e \in \partial T \text{ and } T \in \mathcal{T}_h^1, \\ \lambda_h, & \text{otherwise.} \end{cases} \tag{14}
$$

Introducing the delta function δ_Γ, defined on $\partial\mathcal{T}_h$ as

$$\delta_\Gamma = \begin{cases} 1, & \text{if } e \cap \Gamma \neq \emptyset, \text{ for } e \in \partial T \text{ and } T \in \mathcal{T}_h^1, \\ 0, & \text{otherwise.} \end{cases} \tag{15}$$

and using (14), we can rewrite (12) and (13) as

$$\tfrac{1}{\kappa}\left(\boldsymbol{\sigma}_h, \boldsymbol{\tau}_h\right)_T - \left(u_h, \nabla\cdot\boldsymbol{\tau}_h\right)_T + \langle \lambda_h + \delta_\Gamma s_D, \boldsymbol{\tau}_h\cdot\mathbf{n}\rangle_{\partial T} = 0, \tag{16}$$

$$-\left(\nabla\cdot\boldsymbol{\sigma}_h, v_h\right)_T = -\left(f, v_h\right)_T. \tag{17}$$

Observe that if λ_h is available, we can solve the system (16)-(17) in element level. Hence, (16)-(17) defines a local problem that determines $(\boldsymbol{\sigma}_h, u_h)$ as a function of λ_h on each element.

To determine λ_h we enforce weakly the continuity requirements for the normal component of the flux variable across interelement boundaries and also we impose weakly the Neumann boundary condition. We require that $\lambda_h \in \mathcal{M}_h$ satisfies

$$\langle \boldsymbol{\sigma}_h\cdot\mathbf{n}, \mu_h\rangle_{\partial\mathcal{T}_h\setminus\left(\mathcal{E}_h^D\cup\mathcal{E}_h^N\right)} - \langle s_N, \mu_h\rangle_\Gamma + \langle \boldsymbol{\sigma}_h\cdot\mathbf{n} - g_N, \mu_h\rangle_{\mathcal{E}_h^N} = 0 \quad \forall \mu_h \in \mathcal{M}_h. \tag{18}$$

Finally, summing the equations (16) and (17) over all elements, from (18) and rearranging some terms, we obtain the fitted MHDG formulation for the diffusion interface problem.

3.1. Fitted MHDG method. Find $(\boldsymbol{\sigma}_h, u_h, \lambda_h) \in \mathcal{V}_h \times \mathcal{U}_h \times \mathcal{M}_h$ such that, for all $(\boldsymbol{\tau}_h, v_h, \mu_h) \in \mathcal{V}_h \times \mathcal{U}_h \times \mathcal{M}_h$

$$\begin{cases} \text{(i)} & \tfrac{1}{\kappa}\left(\boldsymbol{\sigma}_h, \boldsymbol{\tau}_h\right)_{\mathcal{T}_h} - \left(u_h, \nabla\cdot\boldsymbol{\tau}_h\right)_{\mathcal{T}_h} + \langle \lambda_h, \boldsymbol{\tau}_h\cdot\mathbf{n}\rangle_{\partial\mathcal{T}_h\setminus\mathcal{E}_h^D} \\ & \quad = -\langle \delta_\Gamma s_D, \boldsymbol{\tau}_h\cdot\mathbf{n}\rangle_{\partial\mathcal{T}_h} - \langle g_D, \boldsymbol{\tau}_h\cdot\mathbf{n}\rangle_{\mathcal{E}_h^D}, \\ \text{(ii)} & -\left(\nabla\cdot\boldsymbol{\sigma}_h, v_h\right)_{\mathcal{T}_h} = -\left(f, v_h\right)_{\mathcal{T}_h}, \\ \text{(iii)} & \langle \boldsymbol{\sigma}_h\cdot\mathbf{n}, \mu_h\rangle_{\partial\mathcal{T}_h\setminus\mathcal{E}_h^D} = \langle s_N, \mu_h\rangle_\Gamma + \langle g_N, \mu_h\rangle_{\mathcal{E}_h^N}. \end{cases} \tag{19}$$

3.1.1. Matrix representation for the fitted MHDG method. The fitted MHDG formulation (19) yields the following (global) linear system

$$\begin{bmatrix} A & B^T & C^T \\ B & 0 & 0 \\ C & 0 & 0 \end{bmatrix} \begin{bmatrix} \boldsymbol{\sigma} \\ \mathbf{u} \\ \boldsymbol{\lambda} \end{bmatrix} = \begin{bmatrix} \mathbf{f_1} \\ \mathbf{f_2} \\ \mathbf{f_3} \end{bmatrix}, \tag{20}$$

where $\boldsymbol{\sigma}$, $\mathbf{u}$ and $\boldsymbol{\lambda}$ correspond to the vector of degrees of freedom for $\boldsymbol{\sigma}_h$, u_h and λ_h, respectively.

For the implementation details of the fitted MHDG method (19), we refer [3] and [9].

3.1.2. Numerical results. The lowest order interpolation finite element spaces $\mathcal{V}_h$, $\mathcal{U}_h$ and $\mathcal{M}_h$ are applied in all numerical tests in this paper. In this section we present numerical results of the performance of the proposed fitted MHDG formulation (19) for the diffusion interface problem (1). To study the convergence of the method, we compute the numerical solutions on a sequence of fitted unstructured refined meshes. The meshes are generated by the mesh generator EasyMesh.

The accuracy of the method is measured by the following relative errors in $L^2(\Omega)$-norm

$$e_\Omega^u = \frac{\|u - u_h\|_{0,\Omega}}{\|u\|_{0,\Omega}}, \quad e_\Omega^{\boldsymbol{\sigma}} = \frac{\|\boldsymbol{\sigma} - \boldsymbol{\sigma}_h\|_{0,\Omega}}{\|\boldsymbol{\sigma}\|_{0,\Omega}}, \tag{21}$$

where $\|\cdot\|_{0,\Omega}$ denotes the $L^2(\Omega)$-norm. We are particularly interested in the accuracy of the method on the interface which can be measured by the following relative errors in $L^2(\Gamma)$-norm

$$e_\Gamma^{u^i} = \frac{\|u^i - u_h^i\|_{0,\Gamma}}{\|u^i\|_{0,\Gamma}}, \quad e_\Gamma^{\boldsymbol{\sigma}^i\cdot\mathbf{n}^1} = \frac{\|(\boldsymbol{\sigma}^i - \boldsymbol{\sigma}_h^i)\cdot\mathbf{n}^1\|_{0,\Gamma}}{\|\boldsymbol{\sigma}^i\cdot\mathbf{n}^1\|_{0,\Gamma}}, \quad i = 1, 2. \tag{22}$$

Test 1. As in Zilian et al. [37], we consider the elliptic interface problem in a square domain $\Omega = (0,1)^2$ with Dirichlet boundary conditions. The domain Ω is partitioned by an immersed interface Γ into an upper subdomain Ω^1 and a lower subdomain Ω^2. In each subdomain the diffusion coefficient κ^i is constant. The problem is defined by

$$\begin{cases} \text{(i)} & \frac{1}{\kappa^i}\boldsymbol{\sigma}^i + \nabla u^i = 0 & \text{in } \Omega^i, \\ \text{(ii)} & \nabla\cdot\boldsymbol{\sigma}^i = f & \text{in } \Omega^i, \\ \text{(iii)} & u^i = g_D & \text{on } \partial\Omega_D \cap \partial\Omega^i, \\ \text{(iv)} & [\![u]\!] = s_D\mathbf{n}^1 & \text{on } \Gamma, \\ \text{(v)} & [\![\boldsymbol{\sigma}]\!] = s_N & \text{on } \Gamma. \end{cases} \tag{23}$$

Let $f = 0$ and the exact solution be as follows:

$$u(x,y) = \begin{cases} \kappa^1 sin(\pi x)\left[cosh(\pi y) - coth(\pi)sinh(\pi y)\right], \\ \qquad\qquad \text{if } x \in \Omega^1, \\ \kappa^2 sin(\pi x)\left[cosh(\pi y) - coth(\pi)sinh(\pi y)\right], \\ \qquad\qquad \text{if } x \in \Omega^2, \end{cases} \tag{24}$$

where $\Omega^1 := \{(x,y) \in \Omega : \phi(x,y) > 0\}$, $\Omega^2 := \{(x,y) \in \Omega : \phi(x,y) < 0\}$ and $\phi(x,y) = y - 1/3$ corresponds to the level set function which defines the interface.

In this test we consider two cases: Case A, $\kappa^1 = \kappa^2 = 1$; Case B, $\kappa^1 = 3$ and $\kappa^2 = 0.5$. We can observe that, in the Case A the exact solution and the normal component of the flux are continuous on the interface, and in the Case B the solution and the normal flux are discontinuous across the interface. The interfacial jump conditions are given by

- Case A:

$$[\![u]\!] = 0, \quad [\![\boldsymbol{\sigma}]\!] = 0 \quad \text{on } \Gamma. \tag{25}$$

- Case B:

$$[\![u]\!] = \left(\kappa^1 - \kappa^2\right) sin(\pi x)\left[cosh(\pi y) - coth(\pi)sinh(\pi y)\right]\mathbf{n}^1 \quad \text{on } \Gamma, \tag{26}$$

$$[\![\boldsymbol{\sigma}]\!] = \pi\left[\left(\kappa^2\right)^2 - \left(\kappa^1\right)^2\right]\begin{bmatrix} cos(\pi x)\left\{cosh(\pi y) - coth(\pi)sinh(\pi y)\right\} \\ sin(\pi x)\left\{sinh(\pi y) - coth(\pi)cosh(\pi y)\right\} \end{bmatrix}\cdot\mathbf{n}^1 \quad \text{on } \Gamma. \tag{27}$$

Figure 3 shows the exact and numerical solutions at the horizontal interface in the cases A and B. These results for the variable u and the normal component $\boldsymbol{\sigma}\cdot\mathbf{n}^1$ of the variable $\boldsymbol{\sigma}$ are obtained on a fitted unstructured mesh with mesh size $h = 0.03125$, consisting of 1281 nodes, 2340 elements and 3710 sides, by evaluating the approximated solutions at the Gauss points of the piecewise linear interface. Very good approximations to both the variables u and the normal component of $\boldsymbol{\sigma}$ on the interface can be observed in both cases. Figures 4 and 5 present the optimal convergence results for the approximations u_h and $\boldsymbol{\sigma}_h$ in $L^2(\Omega)$-norm relative error and in $L^2(\Gamma)$-norm relative error for both cases. We can observe that the proposed method presents very good approximations to all variables globally and near to the interface, for the homogeneous and non-homogeneous interface conditions.

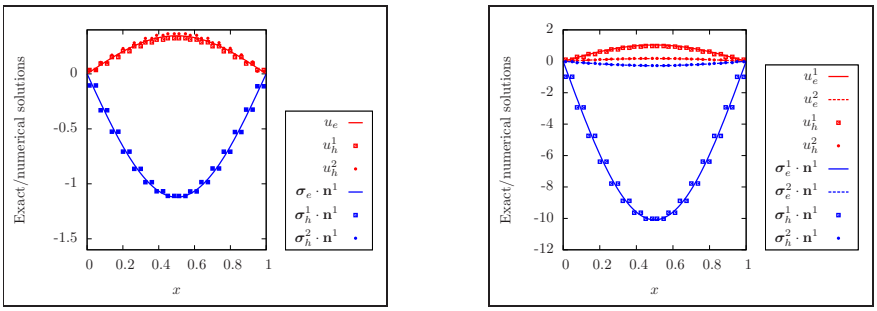

(A) Case A (B) Case B

FIGURE 3. Exact solutions of u and $\boldsymbol{\sigma} \cdot \mathbf{n}^1$ and their numerical solutions at the Gauss points of the horizontal interface $y = 1/3$.

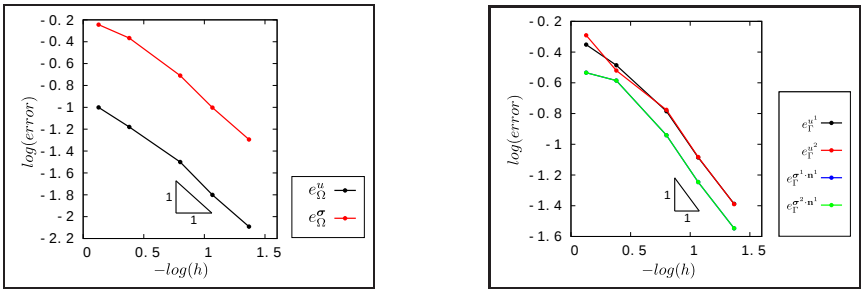

FIGURE 4. Convergence rates for the Case A.

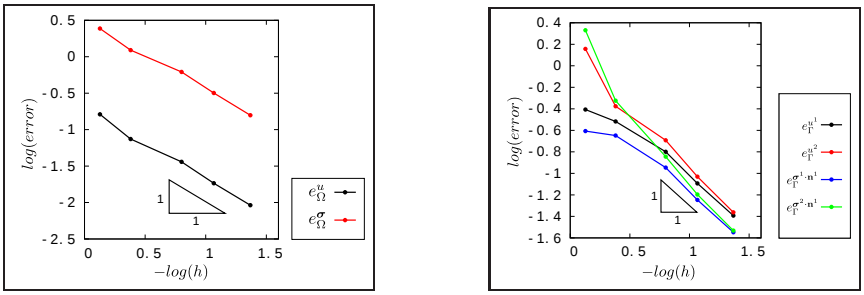

FIGURE 5. Convergence rates for the Case B.

Test 2. In this test, we are interested in the sensitivity of the method (19) for high contrast in material properties. We consider the following problem which is similar to that tested in Annavarapu et al.[1]:

$$
(28)\quad \begin{cases}
\text{(i)} & \frac{1}{\kappa^i}\boldsymbol{\sigma}^i + \nabla u^i = 0 & \text{in } \Omega^i, \\
\text{(ii)} & \nabla \cdot \boldsymbol{\sigma}^i = f & \text{in } \Omega^i, \\
\text{(iii)} & u^i = 1 & \text{on } \partial\Omega_D \cap \partial\Omega^i = \{(x,y) \in \Omega : x = 0, 1\}, \\
\text{(iv)} & \boldsymbol{\sigma}^i \cdot \mathbf{n}^i = 0 & \text{on } \partial\Omega_N \cap \partial\Omega^i = \{(x,y) \in \Omega : y = 0, 1\}, \\
\text{(v)} & [\![u]\!] = s_D \mathbf{n}^1 & \text{on } \Gamma, \\
\text{(vi)} & [\![\boldsymbol{\sigma}]\!] = 0 & \text{on } \Gamma,
\end{cases}
$$

where $\Omega = (0,1)^2$, $f^1 = f^2 = 1$. The exact solution is as follows:

$$u(x,y) = \begin{cases} \dfrac{(3\kappa^1+\kappa^2)x}{4\kappa^1(\kappa^1+\kappa^2)} - \dfrac{x^2}{2\kappa^1} + 1, \\ \qquad \text{if } x \in \Omega^1 = \{(x,y) \in \Omega : \phi(x,y) > 0\}, \\ \dfrac{\kappa^2-\kappa^1+(3\kappa^1+\kappa^2)x}{4\kappa^2(\kappa^1+\kappa^2)} - \dfrac{x^2}{2\kappa^2} + 1, \\ \qquad \text{if } x \in \Omega^2 = \{(x,y) \in \Omega : \phi(x,y) < 0\}, \end{cases} \tag{29}$$

where $\phi(x,y) = c - x$ corresponds to the level set function to define the vertical interface and $c \in \mathbb{R}$ is a parameter to fix the interface location.

Again we use an unstructured mesh with $h = 0.03125$, consisting of 1281 nodes, 2340 elements and 3710 sides. We set $c = 0.8$, $\kappa^1 = 1$ and vary κ^2 from 10^{-6} to 10^6 in terms of a geometric progression with common ratio 10. For each ratio between κ^2 and κ^1 we compute on the interface the relative error in percentage for the variable u as

$$\mathcal{E}_\infty^{u^i} = \max_{(x_p,y_p)\in\Gamma_T, T\in\mathcal{T}_h^0} \left(\frac{|u(x_p,y_p) - u_h^i(x_p,y_p)|}{|u(x_p,y_p)|} \right) * 100, \quad i = 1,2, \tag{30}$$

and for the normal component of the flux variable $\boldsymbol{\sigma}$ as

$$\mathcal{E}_{\infty,\Gamma}^{\boldsymbol{\sigma}^i\cdot\mathbf{n}^1} = \max_{(x_p,y_p)\in\Gamma_T, T\in\mathcal{T}_h^0} \left(\frac{|(\boldsymbol{\sigma}(x_p,y_p) - \boldsymbol{\sigma}_h^i(x_p,y_p))\cdot\mathbf{n}^1|}{|\boldsymbol{\sigma}(x_p,y_p)\cdot\mathbf{n}^1|} \right) * 100, \quad i = 1,2, \tag{31}$$

where $\{(x_p,y_p)\}$ correspond to the Gauss points of integration on the interface Γ_T.

Figure 6 presents very good sensitivities of the variable u and the normal component of the flux variable $\boldsymbol{\sigma}\cdot\mathbf{n}^1$ for large material heterogeneities.

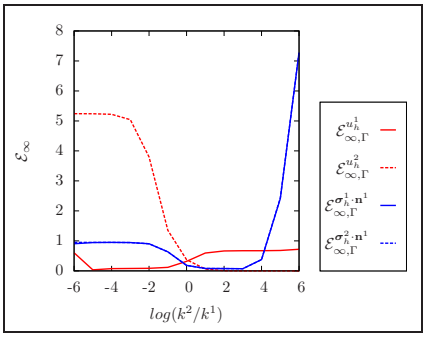

FIGURE 6. Sensitivity for material contrast. Fitted MHDG method.

4. Unfitted MHDG finite element method

We are now going to consider an unfitted partition $\mathcal{T}_h$ of Ω. As in [16] we assume that the mesh satisfies:

- The triangulation $\mathcal{T}_h$ is regular.
- If $\Gamma \cap T \neq \emptyset, T \in \mathcal{T}_h$, then Γ intersects ∂T exactly twice, and each edge at most once.
- Let $\Gamma_{T,h}$ be the straight line segment connecting the point of intersection between Γ and ∂T. We assume that Γ_T is a function of length on $\Gamma_{T,h}$: in particular, in local coordinates (s,t) we have $\Gamma_{T,h} = \{(s,t) : 0 < s < |\Gamma_{T,h}|, t = 0\}$

and $\Gamma_T = \{(s,t) : 0 < s < |\Gamma_{T,h}|, t = \delta(s)\}$, where δ is positive in the direction $\mathbf{n}^1$. This assumption is always fulfilled for sufficiently fine meshes with a bounded curvature Γ.

Multiplying (2.i,ii) by test functions $\boldsymbol{\tau}_h$ and v_h respectively, integrating on element $T \in \mathcal{T}_h$, and applying the Green formula, we obtain

$$\frac{1}{\kappa}(\boldsymbol{\sigma}_h, \boldsymbol{\tau}_h)_T - (u_h, \nabla\cdot\boldsymbol{\tau}_h)_T + \langle \lambda_h, \boldsymbol{\tau}_h\cdot\mathbf{n}\rangle_{\partial T} + \sum_i \langle u_h^i, \boldsymbol{\tau}_h^i\cdot\mathbf{n}^i\rangle_{\Gamma_T} = 0, \tag{32}$$

$$-(\boldsymbol{\sigma}_h, \nabla v_h)_T + \langle \boldsymbol{\sigma}_h\cdot\mathbf{n}, v_h\rangle_{\partial T} + \sum_i \langle \boldsymbol{\sigma}_h^i\cdot\mathbf{n}^i, v_h^i\rangle_{\Gamma_T} = (f, v_h)_T\,, \tag{33}$$

where the integral terms on Γ_T appear only if $T \in \mathcal{T}_h^0$.

Summing over all elements in $\mathcal{T}_h$ we have

$$\begin{aligned}\frac{1}{\kappa}(\boldsymbol{\sigma}_h, \boldsymbol{\tau}_h)_{\mathcal{T}_h} - (u_h, \nabla\cdot\boldsymbol{\tau}_h)_{\mathcal{T}_h} + \langle \lambda_h, \boldsymbol{\tau}_h\cdot\mathbf{n}\rangle_{\partial\mathcal{T}_h\setminus\mathcal{E}_h^D} + \sum_i \langle u_h^i, \boldsymbol{\tau}_h^i\cdot\mathbf{n}^i\rangle_{\Gamma} \\ = -\langle g_D, \boldsymbol{\tau}_h\cdot\mathbf{n}\rangle_{\mathcal{E}_h^D},\end{aligned} \tag{34}$$

$$-(\boldsymbol{\sigma}_h, \nabla v_h)_{\mathcal{T}_h} + \langle \boldsymbol{\sigma}_h\cdot\mathbf{n}, v_h\rangle_{\partial\mathcal{T}_h} + \sum_i \langle \boldsymbol{\sigma}_h^i\cdot\mathbf{n}^i, v_h^i\rangle_{\Gamma} = (f, v_h)_{\mathcal{T}_h}\,. \tag{35}$$

For the terms involving the interface we have the following identities

$$\begin{aligned}\sum_i \langle u_h^i, \boldsymbol{\tau}_h^i\cdot\mathbf{n}^i\rangle_{\Gamma} &= \sum_{T\in\mathcal{T}_h^0} \langle [\![u_h]\!], \{\boldsymbol{\tau}_h\}_w\rangle_{\Gamma_T} + \langle \{u_h\}^w, [\![\boldsymbol{\tau}_h]\!]\rangle_{\Gamma_T} \\ &= \sum_{T\in\mathcal{T}_h^0} \langle s_D\mathbf{n}^1, \{\boldsymbol{\tau}_h\}_w\rangle_{\Gamma_T} + \langle \{u_h\}^w, [\![\boldsymbol{\tau}_h]\!]\rangle_{\Gamma_T},\end{aligned} \tag{36}$$

and

$$\begin{aligned}\sum_i \langle \boldsymbol{\sigma}_h^i\cdot\mathbf{n}^i, v_h^i\rangle_{\Gamma} &= \sum_{T\in\mathcal{T}_h^0} \langle [\![\boldsymbol{\sigma}_h]\!], \{v_h\}^w\rangle_{\Gamma_T} + \langle \{\boldsymbol{\sigma}_h\}_w, [\![v_h]\!]\rangle_{\Gamma_T} \\ &= \sum_{T\in\mathcal{T}_h^0} \langle s_N, \{v_h\}^w\rangle_{\Gamma_T} + \langle \{\boldsymbol{\sigma}_h\}_w, [\![v_h]\!]\rangle_{\Gamma_T}\end{aligned} \tag{37}$$

where the weighted averages on Γ_T, for $T \in \mathcal{T}_h^0$, defined by

$$\begin{aligned}\{\boldsymbol{\sigma}_h\}_w &= w^1\boldsymbol{\sigma}_h^1 + w^2\boldsymbol{\sigma}_h^2, \quad \{\boldsymbol{\sigma}_h\}^w = w^2\boldsymbol{\sigma}_h^1 + w^1\boldsymbol{\sigma}_h^2, \\ \{u_h\}_w &= w^1 u_h^1 + w^2 u_h^2, \quad \{u_h\}^w = w^2 u_h^1 + w^1 u_h^2.\end{aligned} \tag{38}$$

and

$$w^1 = \frac{|T^1|/\kappa^1}{|T^1|/\kappa^1 + |T^2|/\kappa^2}, \qquad w^2 = \frac{|T^2|/\kappa^2}{|T^1|/\kappa^1 + |T^2|/\kappa^2}, \tag{39}$$

satisfy that $w^1 + w^2 = 1$.

Similarly to (18), we require that $\lambda_h \in M_h$ satisfies

$$\langle \boldsymbol{\sigma}_h\cdot\mathbf{n}, \mu_h\rangle_{\partial\mathcal{T}_h\setminus(\mathcal{E}_h^N\cup\mathcal{E}_h^D)} + \langle \boldsymbol{\sigma}_h\cdot\mathbf{n} - g_N, \mu_h\rangle_{\mathcal{E}_h^N} = 0 \quad \forall\mu_h \in \mathcal{M}_h. \tag{40}$$

Thus, we obtain the unfitted MHDG formulation.

4.1. Unfitted MHDG method. Find $(\boldsymbol{\sigma}_h, u_h, \lambda_h) \in \mathcal{V}_h \times \mathcal{U}_h \times \mathcal{M}_h$ such that

(41)
$$\begin{cases} \frac{1}{\kappa}(\boldsymbol{\sigma}_h, \boldsymbol{\tau}_h)_{\mathcal{T}_h} - (u_h, \nabla\cdot\boldsymbol{\tau}_h)_{\mathcal{T}_h} + \langle \lambda_h, \boldsymbol{\tau}_h\cdot\mathbf{n}\rangle_{\partial\mathcal{T}_h\setminus\mathcal{E}_h^D} + \sum_{T\in\mathcal{T}_h^0}\langle \{u_h\}^w, [\![\boldsymbol{\tau}_h]\!]\rangle_{\Gamma_T} \\ \qquad = -\sum_{T\in\mathcal{T}_h^0}\langle s_D\mathbf{n}^1, \{\boldsymbol{\tau}_h\}_w\rangle_{\Gamma_T}, -\langle g_D, \boldsymbol{\tau}_h\cdot\mathbf{n}\rangle_{\mathcal{E}_h^D}, \\ -(\boldsymbol{\sigma}_h, \nabla v_h)_{\mathcal{T}_h} + \langle \boldsymbol{\sigma}_h\cdot\mathbf{n}, v_h\rangle_{\partial\mathcal{T}_h} + \sum_{T\in\mathcal{T}_h^0}\langle \{\boldsymbol{\sigma}_h\}_w, [\![v_h]\!]\rangle_{\Gamma_T} \\ \qquad = (f, v_h)_{\mathcal{T}_h} - \sum_{T\in\mathcal{T}_h^0}\langle s_N, \{v_h\}^w\rangle_{\Gamma_T}, \\ \langle \boldsymbol{\sigma}_h\cdot\mathbf{n}, \mu_h\rangle_{\partial\mathcal{T}_h\setminus\mathcal{E}_h^D} = \langle g_N, \mu_h\rangle_{\mathcal{E}_h^N}, \end{cases}$$

for all $(\boldsymbol{\tau}_h, v_h, \mu_h) \in \mathcal{V}_h \times \mathcal{U}_h \times \mathcal{M}_h$.

The variational formulation (41) can be written equivalently in the following symmetric form:

Find $(\boldsymbol{\sigma}_h, u_h, \lambda_h) \in \mathcal{V}_h \times \mathcal{U}_h \times \mathcal{M}_h$ such that

(42)
$$\begin{cases} \frac{1}{\kappa}(\boldsymbol{\sigma}_h, \boldsymbol{\tau}_h)_{\mathcal{T}_h} - (u_h, \nabla\cdot\boldsymbol{\tau}_h)_{\mathcal{T}_h} + \langle \lambda_h, \boldsymbol{\tau}_h\cdot\mathbf{n}\rangle_{\partial\mathcal{T}_h\setminus\mathcal{E}_h^D} + \sum_{T\in\mathcal{T}_h^0}\langle \{u_h\}^w, [\![\boldsymbol{\tau}_h]\!]\rangle_{\Gamma_T} \\ \qquad = -\sum_{T\in\mathcal{T}_h^0}\langle s_D\mathbf{n}^1, \{\boldsymbol{\tau}_h\}_w\rangle_{\Gamma_T}, -\langle g_D, \boldsymbol{\tau}_h\cdot\mathbf{n}\rangle_{\mathcal{E}_h^D}, \\ -(\nabla\cdot\boldsymbol{\sigma}_h, v_h)_{\mathcal{T}_h} + \sum_{T\in\mathcal{T}_h^0}\langle [\![\boldsymbol{\sigma}_h]\!], \{v_h\}^w\rangle_{\Gamma_T} \\ \qquad = -(f, v_h)_{\mathcal{T}_h} + \sum_{T\in\mathcal{T}_h^0}\langle s_N, \{v_h\}^w\rangle_{\Gamma_T}, \\ \langle \boldsymbol{\sigma}_h\cdot\mathbf{n}, \mu_h\rangle_{\partial\mathcal{T}_h\setminus\mathcal{E}_h^D} = \langle g_N, \mu_h\rangle_{\mathcal{E}_h^N}, \end{cases}$$

for all $(\boldsymbol{\tau}_h, v_h, \mu_h) \in \mathcal{V}_h \times \mathcal{U}_h \times \mathcal{M}_h$.

4.1.1. Implementation of the unfitted MHDG method. For the implementation of the unfitted MHDG method (42), similarly in [2, 3, 9], first, we present the global linear system associated to the discrete formulation and explain the procedure to eliminate the primary variables in terms of the Lagrange multipliers. Then we show how to construct the finite element spaces, and finally, because the formulation is implemented element by element, we also describe the matrix representation at element level with necessary modifications for those cut elements.

The presented implementation technique can be applied for high order interpolations and also for the other unfitted methods presented in the next sections.

4.1.2. Matrix representation for the unfitted MHDG method. The MHDG formulation (42) yields the following (global) linear system

$$\begin{bmatrix} A & B^T & C^T \\ B & 0 & 0 \\ C & 0 & 0 \end{bmatrix} \begin{bmatrix} \boldsymbol{\sigma} \\ \mathbf{u} \\ \boldsymbol{\lambda} \end{bmatrix} = \begin{bmatrix} \mathbf{f_1} \\ \mathbf{f_2} \\ \mathbf{f_3} \end{bmatrix}, \tag{43}$$

where $\boldsymbol{\sigma}$, $\mathbf{u}$ and $\boldsymbol{\lambda}$ correspond to the vector of degrees of freedom for $\boldsymbol{\sigma}_h$, u_h and λ_h, respectively.

Now we are describing the procedure to eliminate the variables $\boldsymbol{\sigma}$ and $\boldsymbol{u}$ in terms of the global variable $\boldsymbol{\lambda}$.

By the first equation of (43), we have

$$\boldsymbol{\sigma} = A^{-1}\left(\mathbf{f_1} - B^T\mathbf{u} - C^T\boldsymbol{\lambda}\right), \tag{44}$$

replacing in the second and third equations, we have

$$\begin{bmatrix} J & L \\ N & O \end{bmatrix} \begin{bmatrix} \mathbf{u} \\ \boldsymbol{\lambda} \end{bmatrix} = \begin{bmatrix} \mathbf{v_1} \\ \mathbf{v_2} \end{bmatrix}, \tag{45}$$

where

$$\begin{array}{lll} J = BA^{-1}B^T, & L = BA^{-1}C^T, & N = CA^{-1}B^T \\ O = CA^{-1}C^T, & \mathbf{v_1} = BA^{-1}\mathbf{f_1} - \mathbf{f_2}, & \mathbf{v_2} = FA^{-1}\mathbf{f_1} - \mathbf{f_3}. \end{array} \tag{46}$$

By the first equation of (45), we obtain

$$\mathbf{u} = J^{-1}\left(\mathbf{v_1} - L\boldsymbol{\lambda}\right), \tag{47}$$

and replacing in the second equation, we obtain the global system for the Lagrange multipliers

$$M\boldsymbol{\lambda} = \mathbf{f}. \tag{48}$$

where $M = O - NJ^{-1}L$ and $\mathbf{f} = \mathbf{v_2} - NJ^{-1}\mathbf{v_1}$.

Since $\mathcal{V}_h$ is a discontinuous finite element space, the matrix A is block diagonal and easy to be inverted element-wisely to yield a block diagonal inverse. Similarly, the matrix J also is block diagonal and can be inverted element by element because $\mathcal{U}_h$ is also a discontinuous finite element space. After solving the global system for the Lagrange multipliers, we can obtain $\mathbf{u}$ from (47) and $\boldsymbol{\sigma}$ from (44) at element level independently.

4.1.3. Construction of the finite element approximation spaces. We present here how to construct the lowest order discontinuous finite element spaces.

Let an arbitrary element $T \in \mathcal{T}_h$, with center of gravity (x_c, y_c) and an arbitrary edge $e \in \mathcal{E}_h \setminus \mathcal{E}_h^D$. For the local Raviart-Thomas space $\mathcal{RT}_0(T)$ we use the basis functions

$$\phi_1^T = (1,0)\,, \qquad \phi_2^T = (0,1) \qquad \text{and} \qquad \phi_3^T = (x - x_c, y - y_c)\,, \tag{49}$$

given in [3].

For the polynomial spaces $\mathcal{P}^0(T)$ and $\mathcal{P}^0(e)$ the basis are given by $\psi^T = 1$ and $\psi^e = 1$, respectively.

If $T \in \mathcal{T}_h^i$, $i = 1, 2$ and $T \notin \mathcal{T}_h^0$, the basis with support on T are: three $\mathcal{RT}_0(T)$ basis, ϕ_1^T, ϕ_2^T and ϕ_3^T, one $\mathcal{P}^0(T)$ basis, ψ^T and three $\mathcal{P}^0(e)$ basis, ψ^{e_i}, ψ^{e_j} and ψ^{e_k}.

If $T \in \mathcal{T}_h^0$, is cut by interface in a triangular and quadrilateral parts (see Figure 7), the basis with support on T are: six $\mathcal{RT}_0(T)$ basis, $\phi_1^{T^i}$, $\phi_2^{T^i}$, $\phi_3^{T^i}$, $i = 1, 2$, two $\mathcal{P}^0(T)$ basis, ψ^{T^1}, ψ^{T^2} and five $\mathcal{P}^0(e)$ basis, $\psi^{e_j^1}$, $\psi^{e_k^1}$, $\psi^{e_i^2}$, $\psi^{e_j^2}$ and $\psi^{e_k^2}$ (or four $\mathcal{P}^0(e)$ basis if T is divided into two triangles).

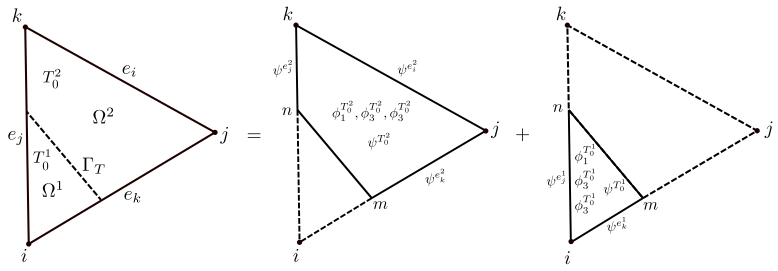

FIGURE 7. Decomposition of element $T_0 \in \mathcal{T}_h^0$, and local bases.

First, for an arbitrary element $T \in \mathcal{T}_h^i$, $i = 1, 2$ and $T \notin \mathcal{T}_h^0$ we have the following local system

$$
\begin{aligned}
&\tfrac{1}{\kappa}\left(\boldsymbol{\sigma}_h, \boldsymbol{\tau}_h\right)_T - \left(u_h, \nabla \cdot \boldsymbol{\tau}_h\right)_T + \langle \lambda_h, \boldsymbol{\tau}_h \cdot \mathbf{n} \rangle_{\partial T \setminus \mathcal{E}_h^D} = -\langle g_D, \boldsymbol{\tau}_h \cdot \mathbf{n} \rangle_{\partial T \cap \mathcal{E}_h^D} \\
&-\left(\nabla \cdot \boldsymbol{\sigma}_h, v_h\right)_T = -\left(f, v_h\right)_T \\
&\langle \boldsymbol{\sigma}_h \cdot \mathbf{n}, \mu_h \rangle_{\partial T \setminus \mathcal{E}_h^D} = \langle g_N, \mu_h \rangle_{\partial T \cap \mathcal{E}_h^N}
\end{aligned} \tag{50}
$$

and the corresponding local matrix representation

$$
\begin{bmatrix} A_T & B_T^T & C_T^T \\ B_T & 0 & 0 \\ C_T & 0 & 0 \end{bmatrix} \begin{bmatrix} \boldsymbol{\sigma}_T \\ \mathbf{u}_T \\ \boldsymbol{\lambda}_T \end{bmatrix} = \begin{bmatrix} \mathbf{f_1}_T \\ \mathbf{f_2}_T \\ \mathbf{f_3}_T \end{bmatrix}, \tag{51}
$$

where the local matrices and vectors have the dimensions: $A_T \in \mathcal{M}_{3\times 3}(\mathbb{R})$, $B_T \in \mathcal{M}_{3\times 1}(\mathbb{R})$, $C_T \in \mathcal{M}_{3\times 3}(\mathbb{R})$, $\mathbf{f_1}_T \in \mathcal{M}_{3\times 1}(\mathbb{R})$, $\mathbf{f_2}_T \in \mathcal{M}_{1\times 1}(\mathbb{R})$ and $\mathbf{f_3}_T \in \mathcal{M}_{3\times 1}(\mathbb{R})$. Appling the procedure described above for the global system. We obtain the local contribution of T to the global system (48).

$$
M_T \boldsymbol{\lambda}_T = \mathbf{f}_T. \tag{52}
$$

Secondly, we consider an arbitrary element $T_0 \in \mathcal{T}_h^0$ consisting of two portions T_0^1 and T_0^2. Figure 8 shows the case when T_0^1 corresponds to the triangular part and T_0^2 is the quadrilateral part of T_0. The triangular part T_0^1 has only two parts of the edges of T_0 while the quadrilateral part T_0^2 has three parts of the edges, so we introduce two and three Lagrange multipliers $(\lambda_{e_j^1}, \lambda_{e_k^1})$ and $(\lambda_{e_i^2}, \lambda_{e_j^2}, \lambda_{e_k^2})$ for T_0^1 and T_0^2 respectively to enforce flux continuities.

For the case when T_0^1 corresponds to the quadrilateral part and T_0^2 is the triangular one, it can be implemented similarly. Then each cut element has five Lagrange multipliers (or four Lagrange multipliers if both T_0^1 and T_0^2 are triangles).

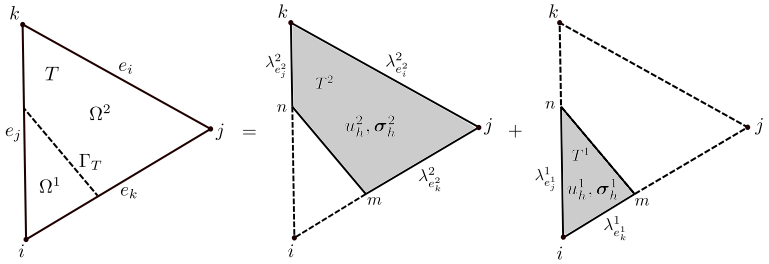

FIGURE 8. Decomposition of element $T_0 \in \mathcal{T}_h^0$. T_0^1 and T_0^2 are the intersections of T_0 with Ω^1 and Ω^2, respectively. Two Lagrange multipliers $(\lambda_{e_j^1}, \lambda_{e_k^1})$ are needed for the triangular part T_0^1 while three Lagrange multipliers $(\lambda_{e_i^2}, \lambda_{e_j^2}, \lambda_{e_k^2})$ are necessary for the quadrilateral part T_0^2.

From (42) we have the local formulation on T_0

$$
\begin{aligned}
&\tfrac{1}{\kappa}\left(\boldsymbol{\sigma}_h, \boldsymbol{\tau}_h\right)_{T_0} - \left(u_h, \nabla \cdot \boldsymbol{\tau}_h\right)_{T_0} + \langle \lambda_h, \boldsymbol{\tau}_h \cdot \mathbf{n} \rangle_{\partial T_0 \setminus \mathcal{E}_h^D} + \langle \{u_h\}^w, [\![\boldsymbol{\tau}_h]\!] \rangle_{\Gamma_{T_0}} \\
&\qquad = -\langle s_D \mathbf{n}^1, \{\boldsymbol{\tau}_h\}_w \rangle_{\Gamma_{T_0}} - \langle g_D, \boldsymbol{\tau}_h \cdot \mathbf{n} \rangle_{\partial T_0 \cap \mathcal{E}_h^D} \\
&-\left(\nabla \cdot \boldsymbol{\sigma}_h, v_h\right)_{T_0} + \langle [\![\boldsymbol{\sigma}_h]\!], \{v_h\}^w \rangle_{\Gamma_{T_0}} = -\left(f, v_h\right)_{T_0} + \langle s_N, \{v_h\}^w \rangle_{\Gamma_{T_0}} \\
&\langle \boldsymbol{\sigma}_h \cdot \mathbf{n}, \mu_h \rangle_{\partial T_0 \setminus \mathcal{E}_h^D} = \langle g_N, \mu_h \rangle_{\partial T_0 \cap \mathcal{E}_h^N}
\end{aligned} \tag{53}
$$

and the corresponding local matrix representation

$$\begin{bmatrix} A_{T_0} & B_{T_0}^T & C_{T_0}^T \\ B_{T_0} & 0 & 0 \\ C_{T_0} & 0 & 0 \end{bmatrix} \begin{bmatrix} \boldsymbol{\sigma}_{T_0} \\ \mathbf{u}_{T_0} \\ \boldsymbol{\lambda}_{T_0} \end{bmatrix} = \begin{bmatrix} \mathbf{f_1}_{T_0} \\ \mathbf{f_2}_{T_0} \\ \mathbf{f_3}_{T_0} \end{bmatrix}, \tag{54}$$

where the element level matrices and vectors have the dimensions: $A_{T_0} \in \mathcal{M}_{6\times 6}(\mathbb{R})$, $B_{T_0} \in \mathcal{M}_{6\times 2}(\mathbb{R})$, $C_{T_0} \in \mathcal{M}_{6\times 5}(\mathbb{R})$ (or $\mathcal{M}_{6\times 4}(\mathbb{R})$), $\mathbf{f_1}_{T_0} \in \mathcal{M}_{6\times 1}(\mathbb{R})$, $\mathbf{f_2}_{T_0} \in \mathcal{M}_{2\times 2}(\mathbb{R})$ and , $\mathbf{f_3}_{T_0} \in \mathcal{M}_{5\times 1}(\mathbb{R})$ (or $\mathcal{M}_{4\times 1}(\mathbb{R})$).

The local contribution of T_0 to the global system (48) is given by

$$M_{T_0}\boldsymbol{\lambda}_{T_0} = \mathbf{f}_{T_0}. \tag{55}$$

We can observe that the local matrix representation is the same for all elements. The difference is the size of the local matrices and vectors.

4.1.4. Numerical results. In this section we focus on the convergence of the unfitted MHDG method (42).

Test 3. We solve the same problem as in Test 1 by the method (42) on the structured meshes.

Figure 9 shows the exact and numerical solutions on the interface. We can observe good approximations to the variable u on both sides of the interface, but to the the normal flux $\boldsymbol{\sigma}\cdot\mathbf{n}$ in both the Cases A and B. Figures 10 and 11 show the convergence results for the Cases A and B, respectively. For the Case A, Figure 10 shows optimal convergence rates for both approximations in $L^2(\Omega)$-norm. For the Case B, Figure 11 shows an optimal convergence rate for the approximation u_h and a suboptimal convergence rate for $\boldsymbol{\sigma_h}$ globally. We observe in the Case B non convergence in $L^2(\Gamma)$-norm of the numerical interfacial flux on both sides.

As the result, the unfitted MHDG method (42) does not work well although it has a good approximation to u. The normal flux on the interface is not well approximated and it is necessary to develop a new unfitted MHDG method.

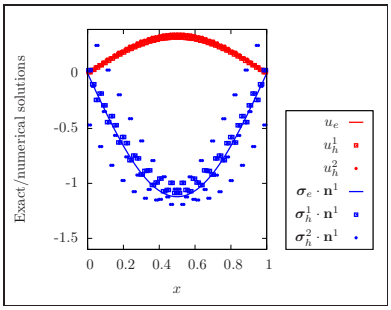

(A) Case A

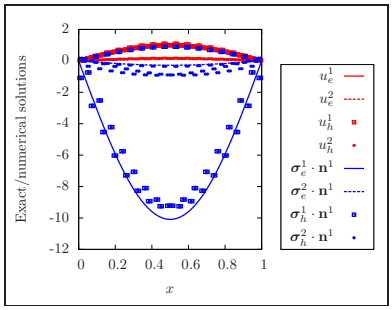

(B) Case B

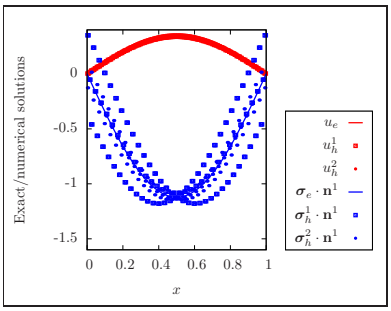

(c) Case A

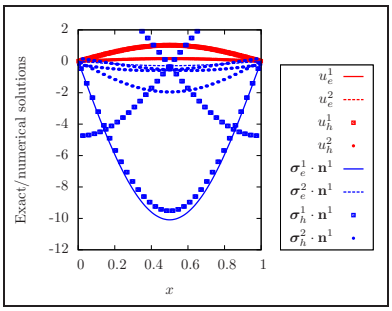

(d) Case B

FIGURE 9. Exact solutions and their numerical solutions at the Gauss points of the interface with structured meshes. (a) and (b) are for the mesh with $h = (1/16)$; (c) and (d) are for the mesh with $h = (1/32)$. Unfitted method (42).

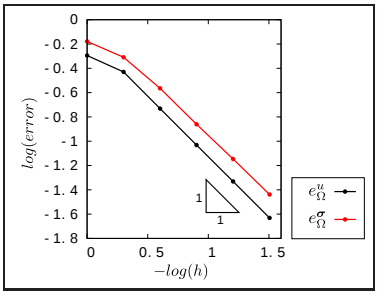

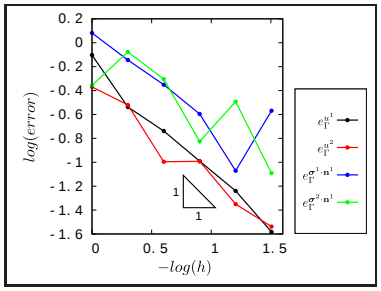

FIGURE 10. Convergence study for the Case A. Unfitted method (42).

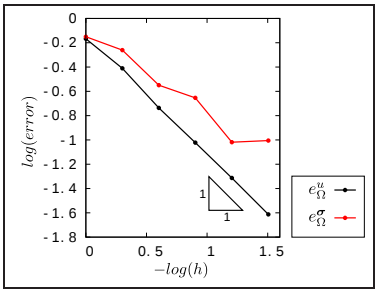

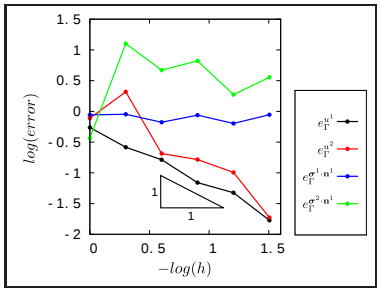

FIGURE 11. Convergence study for the Case B. Unfitted method (42).

4.2. Unfitted MHDG penalty method. The main defect of the method (42) is that two jumps (2.v, vi) on the interface cannot be guaranteed. To do that, we add two penalization terms into the first and second equations of (42) respectively, based on the idea of the Nitsche's penalty method. Then, we have

Find $(\boldsymbol{\sigma}_h, u_h, \lambda_h) \in \mathcal{V}_h \times \mathcal{U}_h \times \mathcal{M}_h$ such that, for all $(\boldsymbol{\tau}_h, v_h, \mu_h) \in \mathcal{V}_h \times \mathcal{U}_h \times \mathcal{M}_h$

(56)
$$
\begin{cases}
\frac{1}{\kappa}\left(\boldsymbol{\sigma}_h, \boldsymbol{\tau}_h\right)_{\mathcal{T}_h} - \left(u_h, \nabla\cdot\boldsymbol{\tau}_h\right)_{\mathcal{T}_h} + \langle \lambda_h, \boldsymbol{\tau}_h\cdot\mathbf{n}\rangle_{\partial\mathcal{T}_h\setminus\mathcal{E}_h^D} + \sum_{T\in\mathcal{T}_h^0}\langle \{u_h\}^w, [\![\boldsymbol{\tau}_h]\!]\rangle_{\Gamma_T} \\
\qquad + \sum_{T\in\mathcal{T}_h^0}\frac{\alpha}{h}\langle [\![\boldsymbol{\sigma}_h]\!], [\![\boldsymbol{\tau}_h]\!]\rangle_{\Gamma_T} \\
\qquad = -\sum_{T\in\mathcal{T}_h^0}\langle s_D\mathbf{n}^1, \{\boldsymbol{\tau}_h\}_w\rangle_{\Gamma_T} + \sum_{T\in\mathcal{T}_h^0}\frac{\alpha}{h}\langle s_N, [\![\boldsymbol{\tau}_h]\!]\rangle_{\Gamma_T} - \langle g_D, \boldsymbol{\tau}_h\cdot\mathbf{n}\rangle_{\mathcal{E}_h^D} \\
-\left(\nabla\cdot\boldsymbol{\sigma}_h, v_h\right)_{\mathcal{T}_h} + \sum_{T\in\mathcal{T}_h^0}\langle [\![\boldsymbol{\sigma}_h]\!], \{v_h\}^w\rangle_{\Gamma_T} + \sum_{T\in\mathcal{T}_h^0}\frac{\beta W_e}{h}\langle [\![u_h]\!], [\![v_h]\!]\rangle_{\Gamma_T} \\
\qquad = -\left(f, v_h\right)_{\mathcal{T}_h} + \sum_{T\in\mathcal{T}_h^0}\langle s_N, \{v_h\}^w\rangle_{\Gamma_T} + \sum_{T\in\mathcal{T}_h^0}\frac{\beta W_e}{h}\langle s_D\mathbf{n}^1, [\![v_h]\!]\rangle_{\Gamma_T}, \\
\langle \boldsymbol{\sigma}_h\cdot\mathbf{n}, \mu_h\rangle_{\partial\mathcal{T}_h\setminus\mathcal{E}_h^D} = \langle g_N, \mu_h\rangle_{\mathcal{E}_h^N},
\end{cases}
$$

where $\alpha, \beta > 0$, and $W_e = \{k\}_w$.

4.2.1. Matrix representation for the unfitted MHDG penalty method. The unfitted MHDG formulation (56) yields the following (global) linear system

$$
\begin{bmatrix} A & B^T & C^T \\ B & D & 0 \\ C & 0 & 0 \end{bmatrix}\begin{bmatrix} \boldsymbol{\sigma} \\ \mathbf{u} \\ \boldsymbol{\lambda} \end{bmatrix} = \begin{bmatrix} \mathbf{f_1} \\ \mathbf{f_2} \\ \mathbf{f_3} \end{bmatrix}, \tag{57}
$$

where $\boldsymbol{\sigma}$, $\mathbf{u}$ and $\boldsymbol{\lambda}$ corresponds to the vector of degrees of freedom for $\boldsymbol{\sigma}_h$, u_h and λ_h, respectively.

The unfitted MHDG formulation (56) maintains the same structure as formulation (42). The penalization terms for u and $\boldsymbol{\sigma}$ are contributed in the matrices A and D, respectively.

4.2.2. Numerical results. Here we evaluate the performance of the unfitted penalty MHDG (56) by its convergences and sensitivities of both interface location and material heterogeneities. For all tests, we consider $\alpha = \beta = 1$.

Test 4. As in Zilian et al. [37], we consider three different shapes of interfaces, see Figure 12. The interfaces are defined by the level set functions

$$
\begin{aligned}
&\phi_1 = y - \tfrac{1}{3}, && \text{(Horizontal interface)} \\
&\phi_2 = y - \tfrac{x}{4} - \tfrac{1}{3}, && \text{(Straight sloped interface)} \\
&\phi_3 = y + x^2 - x - \tfrac{1}{3} && \text{(Curved interface)}
\end{aligned} \tag{58}
$$

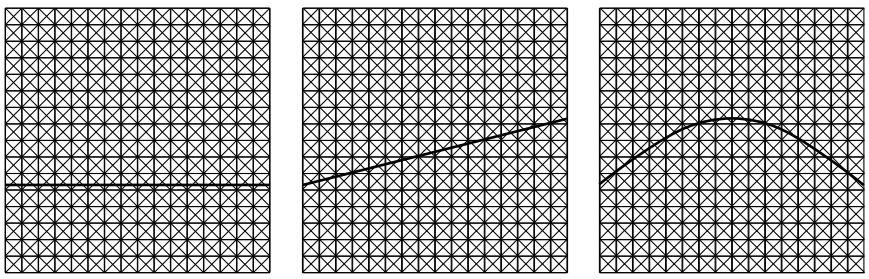

FIGURE 12. Domain geometry and interfaces shape.

The exact and numerical solutions on the horizontal interface shape are presented in Figure 13. It is shown that the introduction of the two penalties produces a significant improvement on the approximation to the interfacial flux. For the Cases A and B, we obtain very good approximations to both u and $\boldsymbol{\sigma}\cdot\mathbf{n}$ on the interface. Figures 14 to 19 show the convergence results of both u_h and $\boldsymbol{\sigma}_h$ for three interface shapes with homogeneous and non-homogeneous jumps. It is observed that the optimal global convergence rates for both u_h and $\boldsymbol{\sigma}_h$ in all of the cases and the interfacial convergence rates are optimal in some cases and suboptimal in the others.

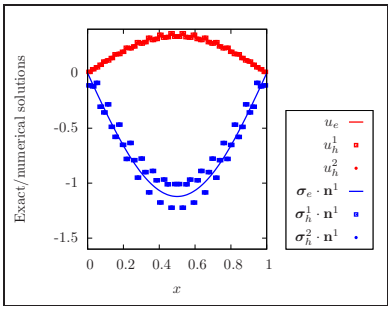

(A) Case A

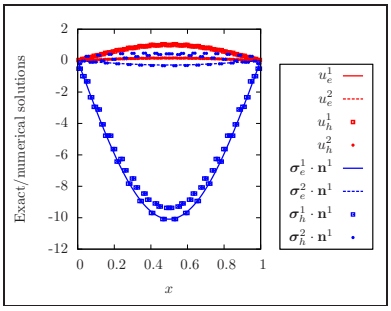

(B) Case B

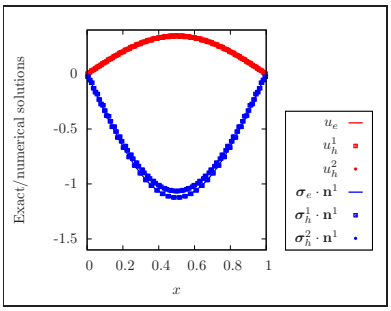

(C) Case A

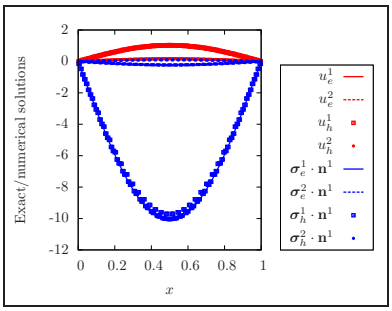

(D) Case B

FIGURE 13. Exact solutions and their numerical solutions at the Gauss points of the horizontal interface on structured meshes. (a) and (b) are for the mesh with $h = (1/16)$; (c) and (d) are for the mesh with $h = (1/32)$. Unfitted MHDG penalty method (56).

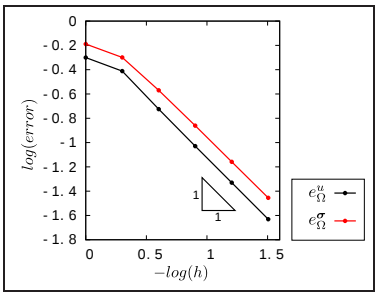

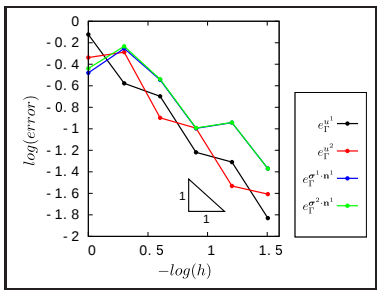

FIGURE 14. Convergence for the horizontal interface. Case A. Unfitted MHDG penalty method (56).

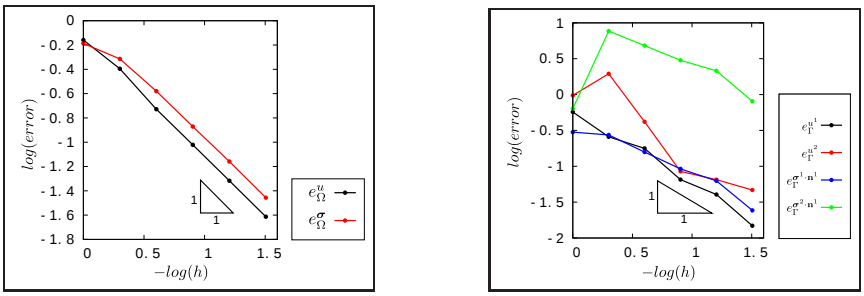

FIGURE 15. Convergence for the horizontal interface. Case B. Unfitted MHDG penalty method (56).

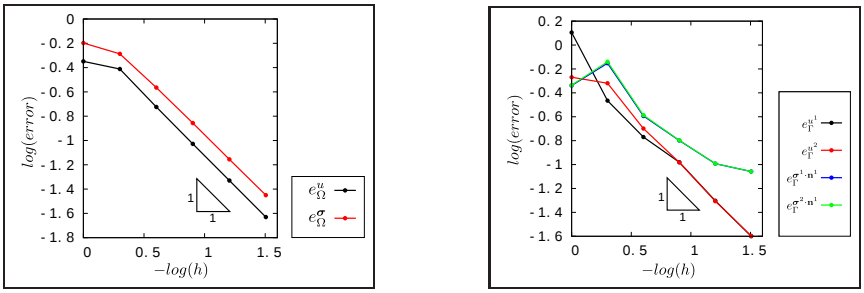

FIGURE 16. Convergence for the sloped interface. Case A. Unfitted MHDG penalty method (56).

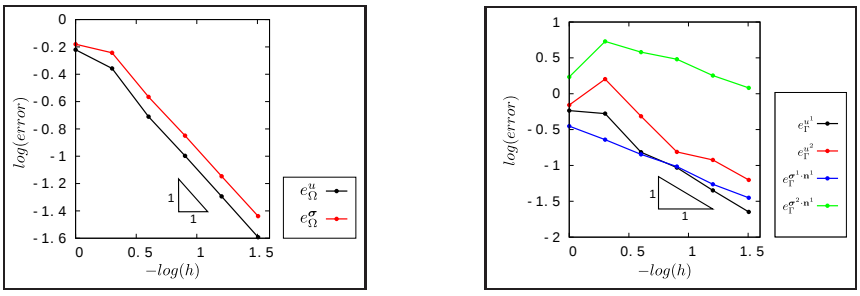

FIGURE 17. Convergence for the sloped interface. Case B. Unfitted MHDG penalty method (56).

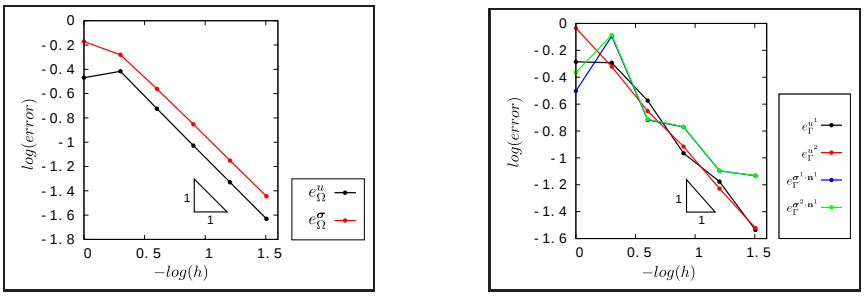

FIGURE 18. Convergence for the curved interface. Case A. Unfitted MHDG penalty method (56).

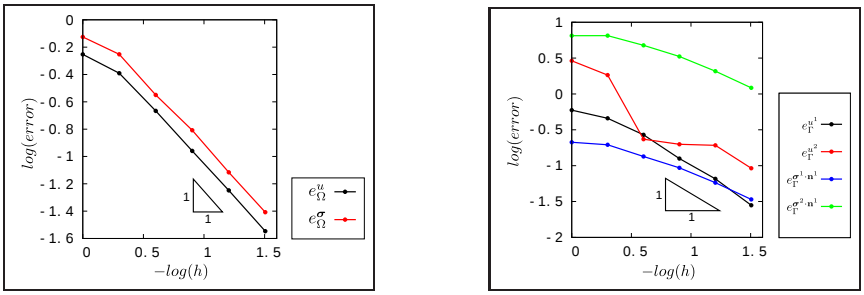

FIGURE 19. Convergence for the curved interface. Case B. Unfitted MHDG penalty method (56).

Test 5. Here we are interested in studying the sensitivity of the unfitted MHDG penalty method (56). We test the robustness of the method in relation to the interface location in a cut element for the same and different material properties. We also evaluate the sensitivity for high contrast in material properties with a fixed interface location.

To study the sensitivity for the interface location, we consider a fixed structured mesh, and we move the interface position from a to b, see Figure 20. For each interface location, we evaluate on the interface the relative maximum error in percentage for u and $\boldsymbol{\sigma}\cdot\mathbf{n}^1$ as in (30) and (31).

In the second part of the test, we fix the interface in the position $x = a+0.13h$ or $x = a+0.87h$. Then we have the level set function $\phi(x, y) = c-x$ with $c = a+0.13h$ or $c = a + 0.87h$. For each position we set $\kappa^1 = 1$, change κ^2 from 10^{-4} to 10^4 in terms of a geometric progression with common ratio 10. For each combination of material properties we compute the relative maximum error in percentage for u and $\boldsymbol{\sigma}\cdot\mathbf{n}^1$.

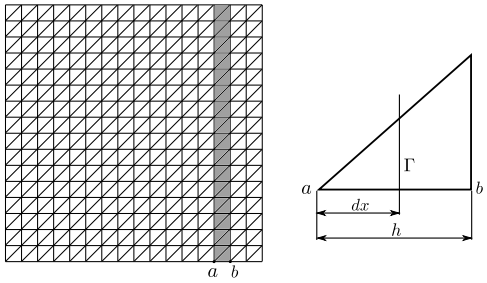

FIGURE 20. Geometry for the sensitivity test used for the unfitted MHDG penalty method (56). The left is the mesh and the right is the parameters for the test.

Figure 21 shows the sensitivity results with respect to the interface location for different material properties. We can observe the very good sensitivities of both u_h and $\boldsymbol{\sigma}_h$ for all combinations of material properties.

Figure 22 shows the sensitivity results for a fixed interface position and variable material diffusivities. The very good sensitivities of both u_h and $\boldsymbol{\sigma}_h$ are also observed for the two considered interface positions.

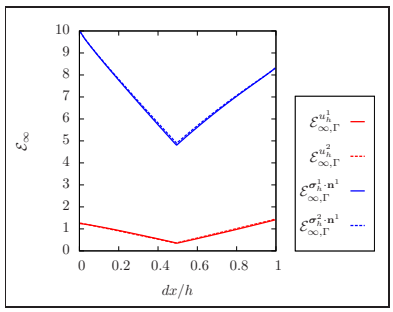

(A) $\kappa^1 = 1$, $\kappa^2 = 1$

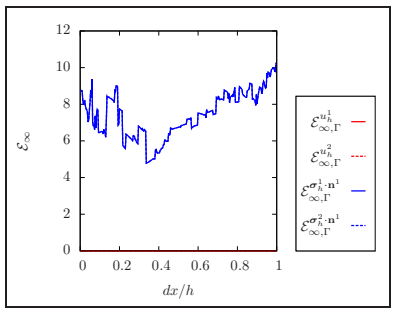

(B) $\kappa^1 = 10^4$, $\kappa^2 = 10^4$

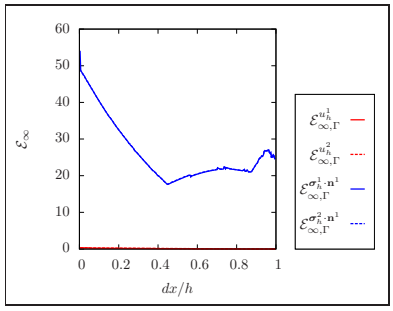

(C) $\kappa^1 = 10^4$, $\kappa^2 = 1$

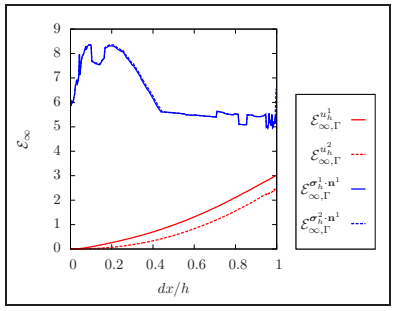

(D) $\kappa^1 = 1$, $\kappa^2 = 10^4$

FIGURE 21. Sensitivity for interface location. Unfitted MHDG penalty method (56).

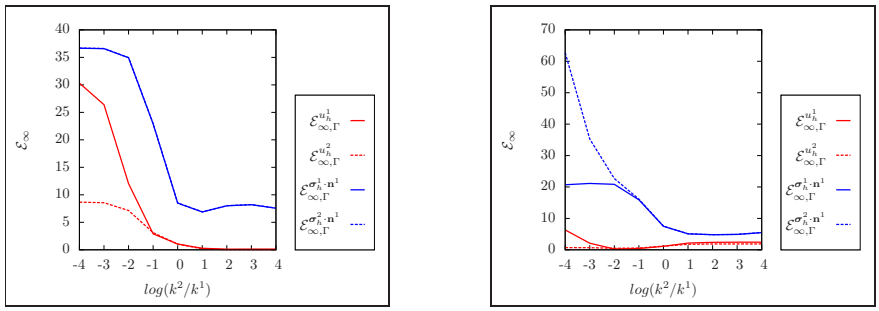

(A) $c = a + 0,13h$ (B) $c = a + 0,87h$

FIGURE 22. Sensitivity for material contrast. Unfitted MHDG penalty method (56).

5. Conclusions and future works

In this paper we propose both fitted and unfitted mixed hybrid discontinuous Galerkin (MHDG) finite element methods to solve numerically elliptic interface problems. The fitted method is a natural application of the classical MHDG for smooth elliptic problems. We present the numerical results on convergences and sensitivities with large material heterogeneities. For the unfitted case, we first propose a MHDG with the *broken* basis functions (unnecessary to satisfy the jump conditions) to those cut elements, and stabilize the method by the weighted averages depending on the volume fractions of cut elements and the material heterogeneities, numerical results show optimal global convergence rate for both the solution and the flux. However the interfacial normal flux is not convergent, and we also observe non-physical oscillations on the cut elements. To solve this problem, we apply the idea of the Nitsche's penalty method to guarantee two jumps on the interface parts of cut elements. Numerical results on convergences and sensitivities of both the interface location within a cut element and the material heterogeneities show that the final unfitted MHDG penalty method is robust and efficient for interface problems. Unlike the immersed interface finite element methods (IIFEM), the two jump conditions are enforced weakly in our variational formulations. So, our unfitted interface MHDG penalty method can be applied more easily than IIFEM to general cases particularly when the immersed basis function cannot be constructed.

In the near future we will give numerical analysis of the proposed unfitted MHDG penalty method and extend to other application problems such as the Darcy flows in fractured porous media, moving interface problems, and so on.

Acknowledgments

J. Zhu's work was supported partially by National Council for Scientific and Technological Development (CNPq) and CAPES of Brazil, and H. Vargas' work was supported by the Doctoral Fellowship from CNPq.

References

[1] C. Annavarapu, M. Hautefeuille and J. E. Dolbow. A robust Nitsche's formulation for interface problems. Comput. Methods Appl. Mech. Engrg. 225-228:44-54, 2012.

[2] D. N. Arnold and F. Brezzi. Mixed and nonconforming finite element methods: implementation, postprocessing and error estimates. RAIRO Modél. Math. Anal. Numér. 19(1):7-32, 1985.

[3] C. Bahriawati and C. Carstensen. Three MATLAB implementations of the lowest-order Raviart-Thomas MFEM with a posteriori error control. Comput. Methods Appl. Math., 5(4):333-361, 2005
[4] T. Belytschko, N. Moös, S. Usui and C. Primi. Arbitrary discontinuities in finite elements. Int. J. Numer. Methods Engng., 50:993-1013, 2001.
[5] C. Bernardi and R. Verfürth. Adaptive finite element methods for elliptic equations with non-smooth coefficients. Numer. Math., 85(4):579-608, 2000.
[6] L. Bevilacqua, R. Feijoo and L. F. Rojas M. A variational principle for the Laplace's operator with application in the torsion of composite rods. Inr. J. Solids Strucrures, 10:1091-1102, 1974.
[7] J. H. Bramble and J. T. King. A Finite element method for interface problems in domains with smooth boundaries and interfaces. Adv. Comput. Math., 6:109-138, 1996.
[8] F. Brezzi, J. Douglas, Jr. and L. D. Marini. Two families of mixed finite elements for second order elliptic problems. Numer. Math., 47:217-235, 1985.
[9] F. Brezzi and M. Fortin. Mixed and Hybrid Finite Element Methods. Springer-Verlag, New York, 1991.
[10] Z. Cai, X. Ye and S. Zhang. Discontinuous Galerkin finite element methods for interface problems: A priori and a posteriori error estimations. SIAM J. Numer. Anal., 49(5):1761-1787, 2011.
[11] B. Cockburn, J. Gopalakrishnan and R. Lazarov. Unified hybridization of discontinuous Galerkin, mixed, and continuous Galerkin methods for second order elliptic problems. SIAM J. Numer. Anal., 47(2):1319-1365, 2009.
[12] H. Egger and J. Schöberl. A hybrid mixed discontinuous Galerkin finite-element method for convection-diffusion problems. IMA J. Numer. Anal., 30:1206-1234, 2010.
[13] B. Fraeijs de Veubeke. Displacement and equilibrium models in the finite element method. In O.C. Zienkiewicz and G. Holister, editors, Stress Analysis. John Wiley and Sons, New York, 1965.
[14] R. P. Fedkiw, T. Aslam, B. Merriman and S. Osher. A non-oscillatory eulerian approach to interfaces in multimaterial flows (the ghost fluid method). J. Comput. Phys., 152(2):457-492, 1999.
[15] Y. Gong, B. Li and Z. Li. Immersed-interface finite-element methods for elliptic interface problems with non-homogeneous jump conditions. SIAM J. Numer. Anal., 46(1):472-495, 2008.
[16] A. Hansbo and P. Hansbo. An unfitted finite element method, based on Nitsche's method for elliptic interface problems. Comput. Methods Appl. Mech. Engrg., 191(47):5537-5552, 2002.
[17] X. He, T. Lin and Y. Lin. A selective immersed discontinuous Galerkin method for elliptic interface problems. Math. Methods Appl. Sci., DOI: 10.1002/mma.2856, 2013.
[18] S. Hou, P. Song, L. Wang and H. Zhao. A weak formulation for solving elliptic interface problems without body fitted grid. J. Comput. Phys., 249:80-95, 2013.
[19] H. Huang and Z. Li. Convergence analysis of the immersed interface method. IMA J. Numer. Anal., 19:583-608, 1999.
[20] L. N. T. Huynh, N. C. Nguyen, J. Peraire and B. C. Khoo. A high-order hybridizable discontinuous Galerkin method for elliptic interface problems. Int. J. Numer. Meth. Engng., 93(2):183-200, 2012.
[21] R. LeVeque and Z. Li. The immersed interface method for elliptic equations with discontinuous coefficients and singular sources. SIAM J. Numer. Anal., 31(4):1019-1044, 1994.
[22] X.-G. Li, J. Zhu, R. Zhang and S. Cao. A combined discontinuous Galerkin method for the dipolar Bose-Einstein condensation. J. Comput. Phys. , 275:363-376, 2014.
[23] Z. Li. The immersed interface method using a finite element formulation. Appl. Numer. Math., 27:253-267, 1998.
[24] Z. Li, T. Lin and X. Wu. New Cartesian grid methods for interface problem using finite element formulation. Numer. Math., 96:61-98, 2003.
[25] X. Liu, R. Fedkiw and M. Kang. A boundary condition capturing method for Poisson's equation on irregular domain. J. Comput. Phys., 160:151-178, 2000.
[26] X. Liu and T. C. Sideris. Convergence of the ghost fluid method for elliptic equations with interfaces. Math. Comp., 72:1731-1746, 2003.
[27] R. Massjung. An unfitted discontinuous Galerkin method applied to elliptic problems. SIAM J. Numer. Anal., 50(6):3134-3162, 2012.
[28] N. Moös, J. Dolbow and T. Belytschko. A finite element method for crack growth without remeshing. Int. J. Numer. Meth. Engng., 46(1):131-150, 1999.

[29] C. S. Peskin. Numerical analysis of blood flow in the heart. J. Comput Phys., 25(3):220-252, 1977.
[30] P. A. Raviart and J. M. Thomas. A mixed finite element method for 2-nd order elliptic problems. In Mathematical aspects of finite element methods, 292-315. Springer Berlin Heidelberg, 1977.
[31] W. H. Reed and T. R. Hill. Triangular mesh methods for the neutron transport equation. Tech. Report No. LA-UR-73-479, Los Alamos Scientific Laboratory, Los Alamos, New Mexico, 1973.
[32] J. Zhang, J. Zhu, X. Yu, A. F. D. Loula and L. Bevilacqua. Mixed finite element analysis of thermally coupled quasi-Newtonian flows. Int. J. Numer. Anal. Model. B, 4(1):35-49, 2013.
[33] J. Zhu and A. F. D. Loula, Mixed finite element analysis of a thermally nonlinear coupled problem. Numer. Methods Partial Differential Eq., 22:180-196, 2006.
[34] J. Zhu, H. Wu and Y. Wang. A mixed method for the mixed initial boundary value problems of equations of semiconductor devices. SIAM J. Numer. Anal., 31(3):731-744, 1994.
[35] J. Zhu, X. Yu and A. F. D. Loula. Mixed discontinuous Galerkin analysis of thermally nonlinear coupled problem. Comput. Methods Appl. Mech. Engrg., 200:1479-1489, 2011.
[36] J. Zhu, J. Zhang, A. F. D. Loula and L. Bevilacqua. Mixed variational formulation and numerical analysis of thermally coupled nonlinear Darcy flows. SIAM J. Numer. Anal., 51(5):2764-2772, 2013.
[37] A. Zilian and T.-P. Fries. A localized mixed-hybrid method for imposing interfacial constraints in the extended finite element method (XFEM). Int. J. Numer. Meth. Engng., 79:733-752, 2009.

Jiang Zhu: Laboratório Nacional de Computação Científica, MCTIC, Avenida Getúlio Vargas 333, 25651-075 Petrópolis, RJ, Brazil

E-mail: jiang@lncc.br and vargaspo@lncc.br